Earth and Planetary Science Letters 280 (2009) 211–219

Contents lists available at ScienceDirect

Earth and Planetary Science Letters

journal homepage: www.elsevier.com/locate/epsl

# Fracturing of volcanic systems: Experimental insights into pre-eruptive conditions

Rosanna Smith *, Peter R. Sammonds, Christopher R.J. Kilburn

*Department of Earth Sciences, University College London, Gower Street, London, WC1E 6BT, UK*

ARTICLE INFO

*Article history:*
Received 20 May 2008
Received in revised form 20 January 2009
Accepted 23 January 2009
Available online 23 February 2009

Editor: R.D. van der Hilst

*Keywords:*
rock mechanics
high temperature fracture
andesite
eruption forecast
VT earthquakes

ABSTRACT

Conditions for fracturing are a primary control on the behaviour of volcanic systems, especially during the approach to eruption. We here present the results of deformation experiments under simulated volcanic conditions on a porhyritic andesite from ancestral Mount Shasta. Andesite was chosen as a representative material because it is common at subduction-zone volcanoes, among both erupted products and country rock. We deformed the lava in tension and triaxial compression tests at strain rates of $10^{-5}$ $s^{-1}$, confining pressures from 0 to 50 MPa and temperatures up to 900 °C. We also concurrently recorded acoustic emissions (AE), in order to monitor cracking activity. The results show that deformation behaviour changes significantly in the temperature range 600–750 °C. Thus, as temperatures increased across this interval, the tensile fracture toughness increased from $2.5 \pm 0.5$ MPa $m^{1/2}$ to $3.5 \pm 1$ MPa $m^{1/2}$, the compressive strength decreased from $110 \pm 30$ MPa to $55 \pm 35$ MPa (at 900 °C) and the corresponding Young's Modulus decreased from $20 \pm 4$ GPa to $6 \pm 4$ GPa. The changes occur when the deformation of the sample changes from elastic–brittle to brittle–ductile behaviour, which we attribute to the blunting of crack tips due to melting of the glass phase and enhanced crystal plasticity at high temperature. AE activity was observed in all experiments, indicating that earthquakes can be generated not only in country rock, but also in hot magma, such as may be found in lava domes and at the margins of magma conduits. In addition, the trends in accelerating AE event rates before sample failure were comparable to those seen in earthquakes before some volcanic eruptions and a minimum in the seismic *b*-value coincided with sample failure. Applied to volcanic systems, the results suggest that (1) andesite strength and elasticity will not be affected by temperature or pressure beyond ~10–100 m from active magma, (2) before eruptions, fractures propagate preferentially through weaker horizons in a mechanically heterogeneous volcano, and (3) volcanic rocks have characteristic seismic *b*-values that are perturbed during the approach to bulk failure. Each of these conditions provides quantitative constraints on models for seismic precursors to eruption or intrusion.



## 1. Introduction

Fractures are a ubiquitous feature of volcanic systems, exerting a fundamental control on the timing of eruptions (Kilburn, 2003; Kilburn and Voight, 1998; Scandone et al., 2007), the stability of domes and volcanic edifices (e.g., Voight and Elsworth, 1997) and the dynamics of lava dome growth and flow emplacement (Fink et al., 1990; Kilburn, 1996; Kilburn, 2004; Smith et al., 2001). The rate of fracturing in the volcanic edifice, recorded as earthquakes, can be used to forecast the timing of eruptions or changes in eruption style (Voight, 1988). In a series of papers, Kilburn and his collaborators developed an eruption forecasting model based on the physics of crack growth (Kilburn, 2003; Kilburn and Sammonds, 2005; Kilburn and Voight, 1998), which Smith et al. (2007) applied to the dome eruption of Mount St. Helens.

Despite the importance of fracturing, few reliable fracture-mechanical data are available for rocks under the pressures and temperatures found at and below volcanoes and of these, most refer to effusive glassy and crystalline basalts (Balme et al., 2004; Hacker and Christie, 1991; Rocchi et al., 2004; Rocchi et al., 2002) and intrusive rocks such as granite and dolerite (Friedman et al., 1979; Meredith and Atkinson, 1985; Murrell and Chakravarty, 1973). In the case of andesites, tensile fracture toughness tests have been conducted at room temperature (Takanohashi and Takahashi, 1986; Waza et al., 1980). Only Bauer et al. (1981) have conducted high temperature triaxial compression tests, at temperatures from 400 to 1050 °C and confining pressures of 50 and 100 MPa, on a fine-grained Mt. Hood andesite, with 10–12% porosity. However, the samples used were 40 mm long × 20 mm in diameter, which provides a ratio of length to diameter that is too small to measure true compressive strengths (ratios >2.5 are required; Paterson, 1978). The restricted nature of the mechanical data sets means that fracture-related models applied to andesitic–dacitic volcanoes normally have to infer relevant mechanical rock properties by analogy with the behaviour of other compositions (e.g., Denlinger, 1990; Hale and Wadge, 2003; Kilburn, 2003).

Acoustic emissions (AE), which are a laboratory scale analogue to seismic events, can be recorded during laboratory deformation

* Corresponding author. Tel.: +44 20 7679 0404; fax: +44 20 7679 2390.
*E-mail addresses:* rosanna.smith@ucl.ac.uk (R. Smith), p.sammonds@ucl.ac.uk (P.R. Sammonds), c.kilburn@ucl.ac.uk (C.R.J. Kilburn).

0012-821X/$ – see front matter © 2009 Elsevier B.V. All rights reserved.
doi:10.1016/j.epsl.2009.01.032

experiments on volcanic rocks, in order to identify the conditions necessary to generate volcanic earthquakes. Although the laboratory AE may have a greater proportion of tensile to shear fractures than expected for volcano-tectonic earthquakes, particularly in uniaxial compression, this is not important when comparing amounts of AE between different temperatures and identifying patterns within an individual experiment. Changes in the AE magnitude distribution characterized by the seismic *b*-value (the negative slope of the log-linear AE frequency–magnitude distribution) have been used to follow the evolution of fracturing (e.g., Sammonds et al., 1992). Most of these studies were conducted at room temperature and few AE data exist for deformation of volcanic rocks at high temperatures (e.g., Smith, 2006). Results from this paper and Tuffen et al. (2008), demonstrate that fracturing in rocks weakened by high temperatures can still generate earthquakes. Previously for andesites, AE data have been obtained only for room temperature experiments (Nishizawa et al., 1984; Rao and Kusunose, 1995) and did not include analyses of changes in AE hit rate or *b*-value.

To rigorously test models of volcano failure and eruption, it is important to investigate the behaviour of appropriate rock types at volcanically-relevant pressures and temperatures. This paper presents the results of fracture-mechanical experiments on andesite in compression and tension, at temperatures up to 900 °C and confining pressures up to 50 MPa (equivalent to depths of about 2 km). Concurrently we have recorded acoustic emissions (AE) to monitor and analyze cracking activity. Applied to an eruption forecasting model (Kilburn, 2003), the results demonstrate that seismic events before the first eruption after a long repose interval are dominated by fracturing in pre-existing zones of weaker rocks, or rocks weakened by higher temperatures.

## 2. Patterns of seismic events at subduction-zone volcanoes

Patterns of volcano-tectonic (VT) seismicity reflect how populations of fractures grow and interact within a volcano. They are therefore commonly used to investigate conditions that may lead to an eruption or to changes in style of eruption, as a result of changes in the stress field within and below a volcanic edifice (Kilburn, 2003; Roman et al., 2006). Thus, before eruptions after long repose, rates of VT seismicity at subduction-zone volcanoes have been observed (1) to accelerate in a systematic manner that yields the potential for forecasting the eruption days ahead of time (Kilburn, 2003; Kilburn and Sammonds, 2005; Voight, 1988), and (2) to show changes in their magnitude–frequency distribution, measured by the seismic *b*-value, as much as months beforehand (Main, 1987; McNutt, 2005). During eruptions, VT and 'hybrid' earthquakes (with a mixture of VT and low frequency earthquake characteristics) may also be produced by the fracturing of chilled magma along the margins of conduits (Neuberg et al., 2006; Tuffen et al., 2008). This feature can be used to monitor changes in magma pressure and flow rate in a conduit at depth, so yielding the additional potential for forecasting accelerations in eruption rate, especially during periods of lava-dome effusion (Roman et al., 2006).

In all cases, the detected events have typical Richter magnitudes less than 2. In the case of dome emplacement they occur within about 2 km below and laterally away from the vent and possibly within the dome itself (Aspinall et al., 1998; Fremont and Malone, 1987; Neuberg et al., 2006). During unrest after long repose intervals, the volume involved in fracturing may extend to depths of about 5 km and radii of 3 km (Aspinall et al., 1998; Nakada et al., 1999). The pressures and temperatures at which detected fracturing occurs may thus range from ambient surface values to about 125 MPa (5 km depth) and 900 °C (for partially molten andesite).

Accelerations in VT event-rate have been interpreted in terms of local changes in strain around fractures, caused by movements along neighbouring fractures (Kilburn and Voight, 1998; McGuire and Kilburn, 1997). Changes in *b*-value can also be related to fracture interaction, because *b*-values have been shown theoretically and empirically to be inversely proportional to the average stress intensity at fracture tips (Main et al., 1993; Meredith and Atkinson, 1983). Stress intensity, in turn, increases with fracture length and the remotely applied stress. Among a population of fractures, therefore, the average stress intensity per fracture is expected to increase, and the *b*-value to decrease, as the fractures grow and coalesce (Main, 1987; McNutt, 2005; Meredith and Atkinson, 1983; Sammonds et al., 1992). Hence, to improve interpretations of changing patterns of volcano seismicity at subduction-zone volcanoes, new data are required on the fracture strengths and moduli of elasticity of andesite in compression and tension, as well as on the interaction of fractures before bulk failure, at temperatures up to 900 °C and confining pressures to at least 50 MPa (2 km depth).

## 3. High temperature rock deformation conditions and procedures

### 3.1. Experimental conditions

Fig. 1 shows the parts of the volcanic system represented by the different experimental methodologies and conditions tested in the laboratory. For positions labelled "1", tensile fracturing is the dominant mode of failure. Rock fails catastrophically in tension when the stress intensity at the tip of a crack equals or exceeds a critical value known as the fracture toughness, $K_c$, (Irwin, 1958). This is simulated in the laboratory by mode I (tensile opening) fracture toughness experiments in both dry unconfined and water saturated confined conditions (with 2 MPa pore pressure and confining pressure). These are conducted at temperatures from atmospheric (representing the surface of old domes) to 900 °C (representing the interior of active domes). For the positions labelled "2", uniaxial and triaxial compression experiments at 900 °C model high temperature fracturing under compressive stresses within the lava dome, at the margins of extruding lava and the underlying crater floor, and the interface between the ascending magma and the conduit walls. For

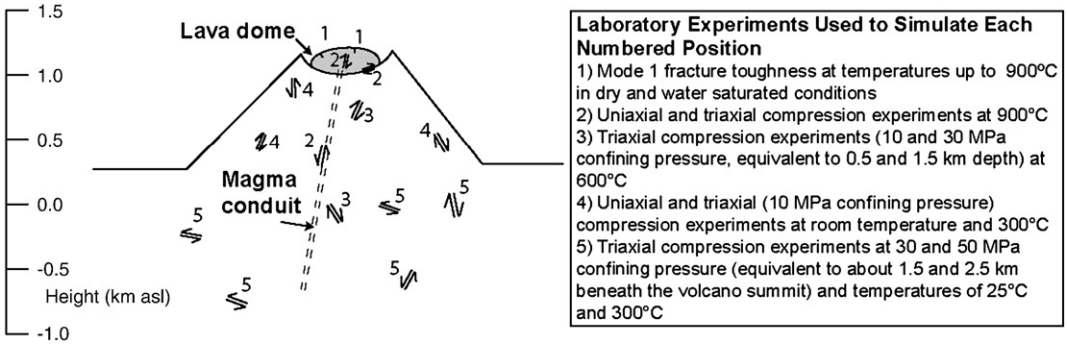


**Fig. 1.** Diagram to show the parts of a volcanic system that rock deformation experiments represent.

the positions labelled "3", triaxial compression experiments (with 10 MPa and 30 MPa confining pressure, which is equivalent to 0.5 and 1.5 km depth) at 600 °C model material fairly close to the conduit (within 10 s of m) deforming in shear mode under compressive stresses. For the positions labelled "4", uniaxial and triaxial (10 MPa confining pressure) compression experiments at room temperature and 300 °C represent fracture of shallow rocks (<500 m) that are not heated or are only minimally heated by the presence of magma. For the positions labelled "5", triaxial compression experiments with confining pressure of 30 and 50 MPa at room temperature and 300 °C represent shear fracture at depths of 1.5 to 2.5 km in material that has only been minimally heated by the presence of magma. Similar conditions have been tested for a Vesuvian phono-tephrite and an Etnean trachybasalt in Rocchi et al. (2004) and are compared in the discussion.

### 3.2. Sample description

The sample of andesite from ancestral Mount Shasta used for the experimental program was collected from an unweathered old lava flow exposed in a road cut on Mount Shasta, a Cascade volcano in Northern California, USA [41N19.90, 122W14.76, 1740 masl]. This andesite is porphyritic with 17% phenocrysts, 83% groundmass, 7.2% porosity, and <1% glass phase. The phenocrysts sizes are 0.3 to 2.5 mm, whilst crystals in the groundmass are less than 0.1 mm. Table 1 shows the bulk composition of this rock with that of the samples tested in Rocchi et al. (2004) and their mineralogy is in the supplementary data in the Appendix. The composition of the Shasta sample is within the andesite classification. Whilst modern andesites from Mount Shasta have high amounts of MgO (3.5 to 5.0%; Grove et al., 2005), this andesite contains only 2–3%, which is within the typical range for andesites (Winter, 2001). This makes it an ideal representative for active lava dome rocks and rocks within the edifices of subduction zone volcanoes. The block taken for experiments had no distinct fractures, faults, anisotropy, or fabric. Blocks from this location have K/Ar ages of 593 ka (Kelley et al., 1987). Examination of thin sections cut in 3 orthogonal directions did not reveal any anisotropy. P and S wave velocities measured in these directions showed anisotropy of <3% (Smith, 2006).

When a rock is heated, differential and anisotropic expansion of crystals induce a population of microcracks. Acoustic emissions and changes in the physical properties and strength of the rock with temperature thus arise due to both the test temperature and this additional cracking. However, on successive heating cycles, a thermal 'kaiser' effect is expected, whereby there is minimal further thermal damage, cracking and thus acoustic emissions unless the previous maximum temperature is exceeded (Fredrich and Wong, 1986). Heat treatment of all samples to a temperature greater than the experimental temperature thus removed all acoustic emissions related to thermal stresses and induced the level of damage expected in the field from slow heating of rocks to the test temperatures. Temperatures should be increased slowly during heat treatment in order to induce microcracking only from the thermal expansion mismatch of the different crystals in the sample, and not from thermal gradients. After specimens had been cored and ground to the geometries described in the next section, they were heat treated by bringing them up to their heat-treatment temperature at 1 °C/min, holding them at this temperature for 1 h, and then cooling them to room temperature at the same rate. For each experiment, the heat treatment temperature was 50 °C higher than the experiment temperature. Changes in acoustic velocities and physical properties of the samples with heat treatment are shown in the supplementary data in the Appendix. After heat treatment, samples for both types of experiment (fracture toughness and compression) were kept in an oven at 70 °C in order to keep them dry. The fracture toughness samples tested in a water saturated environment were saturated with water by leaving them submerged in water in a vacuum chamber for several days before the experiments.

**Table 1**
Bulk composition of ancestral Mount Shasta andesite sample used in this study, and Vesuvian and Etnean lava samples used in Rocchi et al. (2004) for comparison.

| Sample | Ancestral Mount Shasta andesite | Vesuvius 1834 phono-tephrite flow | Etna 1983 trachybasalt flow |
|---|---|---|---|
| $SiO_2$ | 61.1 | 47.8 | 47.3 |
| $TiO_2$ | 0.8 | 1.0 | 1.7 |
| $Al_2O_3$ | 18.2 | 17.6 | 16.7 |
| $Fe_2O_3$ | 6.0 | 3.2 | 11.2 |
| FeO | n.a | 5.0 | n.a |
| MnO | 0.1 | 0.2 | 0.2 |
| MgO | 2.3 | 4.1 | 5.8 |
| CaO | 5.6 | 9.3 | 10.3 |
| $Na_2O$ | 3.6 | 2.6 | 3.8 |
| $K_2O$ | 1.6 | 7.2 | 1.9 |
| $P_2O_5$ | 0.2 | 0.9 | 0.6 |
| $CO_2$ | 0.0 | 0.0 | n.a |
| F | 0.0 | 0.2 | n.a |
| Cl | 0.0 | 0.5 | n.a |
| BaO | 0.1 | n.a | n.a |
| Total | 99.6 | 99.7 | 99.5 |

### 3.3. Triaxial and uniaxial deformation tests

A high temperature triaxial deformation cell, designed and built at University College London and described in Rocchi et al. (2004), was used to deform andesite at temperatures up to 900 °C in uniaxial compression and triaxial compression, at confining pressures up to 50 MPa. The cell incorporates a pressure vessel (500 mm long, by 96 mm internal diameter) pressurised with nitrogen or argon gas using an air-driven gas booster: it has a working pressure limit of 100 MPa and is equipped with an insulated internal heater. Axial load is applied to test samples by a servo-hydraulic actuator which incorporates an internal load cell. The rate of sample shortening or loading is controlled by a new digital servo-control system which employs LABView data acquisition and control software. Attached to the lower deformation piston is an acoustic emission wave guide (Rocchi, 2002). This is a long, stiff metal rod that transmits acoustic waves from the sample to a ceramic piezoelectric transducer. The use of a waveguide attenuates acoustic waves, but as it reduces all amplitudes by the same factor the amplitude distribution of AE events is unaffected (Meredith and Atkinson, 1983).

Cylindrical rock samples, cored to 25 mm diameter and cut to 75 mm long (with ends ground parallel and flat to within 0.01 mm) were employed. These dimensions are large enough to provide valid mechanical data for andesites with phenocrysts of up to 3 mm (diameter >8× phenocryst sizes) and the length: diameter ratio is small enough to prevent buckling and large enough to allow the central section to deform homogeneously (Rocchi et al., 2004). Samples are jacketed in thin, ductile iron or aluminium sleeves (depending on the temperature of the experiment) and insulated by ceramic discs. At 900 °C the temperature gradient along the length of the sample is less than 10 °C. With high confining pressures, convection within the pressure vessel results in high temperatures near the internal load cell (at the top of the vessel). An air cooling system is employed intermittently to cool the load cell (inside) for the highest temperatures, but the noise masks the recording of acoustic emissions.

The following experimental procedure was employed. After heat treatment, the jacketed rock sample was placed inside the pressure vessel and then pressurised. It was heated to the test temperature at a rate of 5 °C/min and then held for 30 min to equilibrate. The test strain rate was selected within LABView and the ramp function generator set to move the actuator and deform the sample at the desired rate. Uniaxial and triaxial compression experiments were conducted under axial strain rate control, at a strain-rate of $10^{-5}\,s^{-1}$. This is slow enough to observe changing stress: strain relationships

and acoustic emission patterns, but fast enough for the experimental conditions to be maintained for the duration of the test. Although this strain rate is considerably higher than those typical of crustal faults ($10^{-15}$ to $10^{-12}$ $s^{-1}$), it is within the range of strain rates observed in lava domes and inferred along the margins of magma conduits (Rust et al., 2003; Beeler et al., 2005).

### 3.4. Fracture toughness tests

Level I fracture toughness experiments at temperatures up to 900 °C were done using the same pressure vessel but with a different sample loading arrangement and furnace (described in Balme et al., 2004). We used the chevron notched short rod sample configuration recommended by the ISRM (1988). In this set up, the pre-cut axial notch is stressed perpendicular to the notch.

The following experimental procedure was employed. Samples were 60 mm diameter cores ground to the recommended geometry to an accuracy of ±0.01 mm. A sample was placed into the cell such that the knife edges of the internal actuator located into the groove in the sample. Pressure in the actuator, controlled with a hand pump, was increased to approximately 5% of the anticipated failure stress of the sample to hold it in place. The pressure vessel with its internal heater was then lowered down over the sample. For the experiments in a water environment, the pressure vessel was filled with water. The sample was then heated to its test temperature at 5 °C/min. Small amounts of steam were vented once the temperature reached 100 °C to keep the pressure at the required test pressure. Once the sample reached its test temperature (whether in air or water) it was left for 30 min to equilibrate. The sample temperature was controlled to within 5 °C for experiments in air and 10 °C for experiments in water. Once the temperature had stabilised, the actuator was loaded using a hand pump until the sample failed (the fracture extends all the way through the sample) whilst recording the force applied to the sample. The fracture toughness was calculated from the applied force and the geometry of the sample.

## 4. Results

### 4.1. Mechanical properties

Fig. 2 shows the fracture toughness against temperature for all tests, with the experiments conducted in water indicated. In dry conditions at temperatures up to 600 °C, the fracture toughness is 2.5 ± 0.5 MPa $m^{1/2}$, with no temperature dependence. This increases to 4.0 ± 0.6 MPa $m^{1/2}$ at 750 °C, then drops to 3.5 ± 1 MPa $m^{1/2}$ at 900 °C. Results were less consistent at 900 °C than any other temperature for dry samples. In water saturated conditions, the fracture toughness remained within this range at 150 °C and dropped to 1.7 ± 0.2 MPa $m^{1/2}$ at 200 °C.

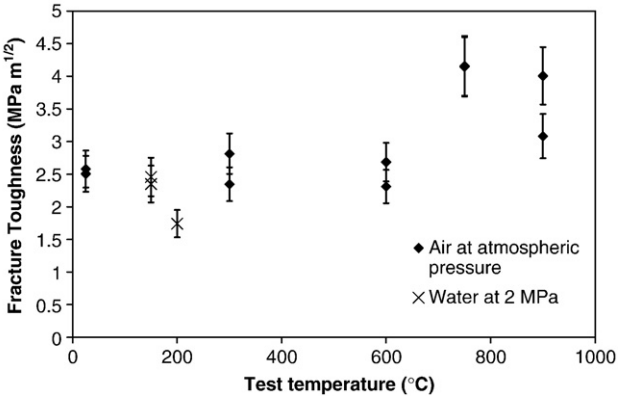


**Fig. 2.** Fracture toughness of ancestral Mount Shasta andesite against temperature. Samples were tested in air under atmospheric pressure, and in water under 2 MPa of confining pressure.

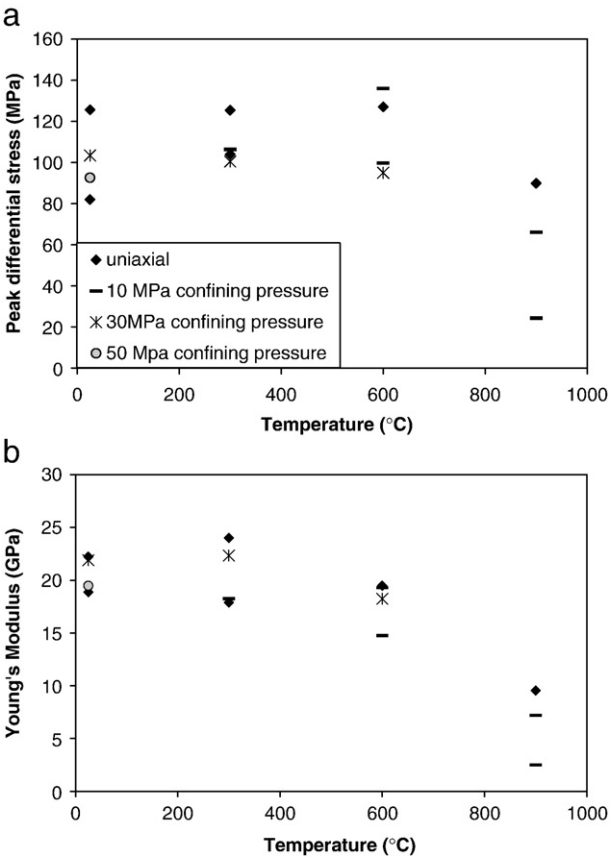


**Fig. 3.** a) Peak differential compressive stresses and b) Young's Modulus, during uniaxial and triaxial deformation tests on ancestral Mount Shasta andesite, plotted against test temperature. Different symbols denote different temperatures and loading conditions. All tests had a strain rate of $10^{-5}$ $s^{-1}$.

Fig. 3 shows the peak differential stress and the Young's Modulus for all compression experiments (some stress strain curves are also described in Section 4.2). From 25 °C to 600 °C, the peak differential stress remained approximately constant at 110 ± 30 MPa. The range in values, attributed to sample variability, is approximately an order of magnitude greater than the individual measurement errors. The Young's Modulus was 21 ± 4 GPa at 25 and 300 °C, dropping slightly to 18 ± 2 MPa at 600 °C. At 900°C the peak differential stress ranged from 24 to 90 MPa and the Young's Modulus was between 2.5 and 9.5 GPa. At this temperature the rock was in the brittle–ductile transition regime and the temperature errors were ±5 °C for uniaxial tests and ±10 °C for triaxial tests. There was no increase in peak differential stress with confining pressure up to 50 MPa.

In each of the three samples deformed at 900 °C, a shear fracture was formed in addition to some barrelling of the samples deformed with 10 MPa confining pressure (Fig. 4). The fracture dissected samples ST45 and ST43, whilst sample ST20 (deformed with 10 MPa confining pressure) remained in one piece. Therefore the visible fracture on sample ST20 either did not penetrate through the whole sample, or welded back together. After the experiment was complete, the differential axial stress was immediately removed, but the confining pressure was not vented until 3 h later, when the temperature had dropped enough. The fracture could have welded back together in this time. SEM images of the surfaces of the through-going shear fractures of samples ST45 and ST43 revealed brittle–ductile textures, evident in the glass on the fracture surface of sample ST43 and quenched melt found on the surface of the fracture in sample ST45 (Tuffen et al., 2008).

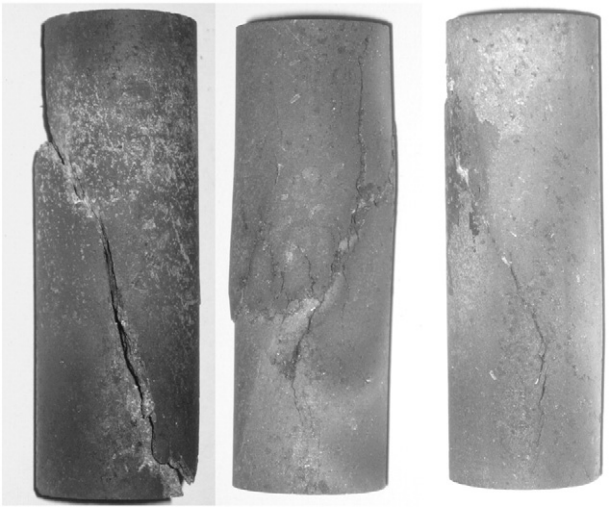

**Fig. 4.** Photographs of the samples deformed in uniaxial and triaxial compression at 900 °C and $10^{-5}$ $s^{-1}$. Sample ST45 (left) was deformed in uniaxial compression and samples ST20 (centre) and ST43 (right) were deformed with 10 MPa confining pressure. Note that a shear fracture formed in all three samples. Samples ST45 and ST43 were dissected along this fracture, but sample ST20 (centre) was not. The samples deformed in triaxial compression (ST20 and ST43, centre and right) also exhibited some barrel shaped bulging.

### 4.2. Acoustic emissions

For all samples where AE were recorded, the amplitude–frequency distribution was fractal through more than two orders of magnitude (see example of power law relationship in Fig. 5). The decibel scale used to report these AE amplitudes is equivalent to the magnitude scale commonly used to calculate *b*-values if the amplitudes are divided by 20 (Cox and Meredith, 1993). This allows analysis of changes in *b*-value during the experiments. The *b*-values were calculated using Aki's (1965) method for 200 hits at 100 hit intervals. This number of hits and dynamic range (two orders of magnitude, a factor of 100) are sufficient for calculating reliable *b*-values from this method. Sample failure coincided with the peak in AE hit rate and a decrease of 0.1 to 0.6 in the *b*-value for all experiments (Table 2). This was also found in previous studies of AE during compression of dry crystalline igneous rocks (Meredith et al., 1990; Thompson et al., 2006). Fig. 6 shows these results in more detail for samples ST14 (deformed at room temperature with 30 MPa confining pressure), ST33 (10 MPa confining pressure at 300 °C), ST42 (10 MPa confining pressure at 600 °C) and ST45 (uniaxial compression at 900 °C). For samples ST14, ST33, and ST42 (deformed in triaxial compression at temperatures from 25 °C to 600 °C) the behaviour was very brittle with elastic deformation until the moment of peak stress and dynamic failure. In these three cases, AE hit rates accelerated in the final stages of sample loading, whilst the *b*-value dropped to its minimum value when the sample failed (at the stress drop). During post-failure frictional sliding, the *b*-value recovered to a similar (samples ST14 and ST42, Fig. 6a and c) or higher (sample ST33, Fig. 6b) value to that recorded during sample loading.

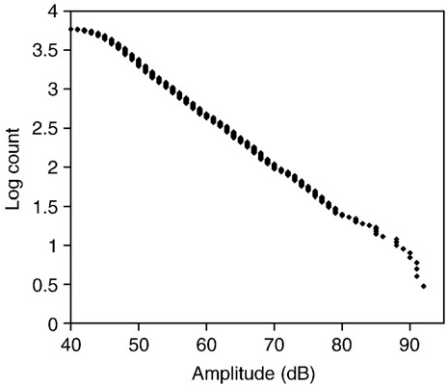


**Fig. 5.** Frequency–amplitude distribution of acoustic emissions recorded during room temperature uniaxial compression of ancestral Mount Shasta andesite. The linear relationship through more than two orders of magnitude (a factor of 100, from 45dB to 85 dB) shows that the amplitude scaling is fractal, so *b*-values can be calculated for this data.

The behaviour of sample ST45 was less brittle than the other three samples shown in Fig. 6, with significant strain hardening (between the yield stress and the peak stress) and strain softening (between the peak stress and dynamic failure) inelastic deformation of 0.37% and 0.06% axial strain respectively. The earlier onset of inelastic deformation was accompanied with an earlier onset of AE than the other samples. There was also a double minimum in the *b*-value, coinciding with the peak stress and dynamic failure of the sample, with the recovery to a higher *b*-value during strain softening deformation.

## 5. Discussion

### 5.1. Brittle deformation

At temperatures up to 600 °C, there was no temperature dependence of the compressive strength or Young's Modulus of ancestral Mount Shasta andesite when deformed at $10^{-5}$ $s^{-1}$, nor its mode I fracture toughness (Figs. 2 and 3). This lack of temperature dependence is relevant to many volcanic systems, given that strain rates are typically from $10^{-7}$ $s^{-1}$ to $10^{-4}$ $s^{-1}$ (Beeler et al., 2005; Rust et al., 2003; Tuffen et al., 2003). The surrounding rocks are also only likely to exceed 600 °C at depths greater than those considered here (up to 5 km) unless they are within 10 s of m of hot molten magma, given typical thermal diffusivities of volcanic rocks of $10^{-7}$ to $10^{-6}$ $m^2$ $s^{-1}$ (Friedman et al., 1981; Lore et al., 2000). Confining pressures up to 50 MPa also had no influence on the compressive strength and Young's Modulus (Fig. 3). This has also been found for basaltic rocks tested on this apparatus at confining pressures up to 30 MPa (Rocchi et al., 2004). This lack of confining pressure influence indicates that these rock types have a high cohesive strength compared with their internal friction, which is expected for a low porosity crystalline rock where the confining pressures are not sufficient to stiffen the rock or inhibit fracture growth. These pressures are equivalent to depths of up to 2 km. The weaker than expected nature of samples deformed at higher pressures, which was particularly evident at higher temperatures, could also be attributed to the increased activity and concentration of water in the glass phase at higher confining pressures.

**Table 2**
Acoustic emission statistics for all compression experiments.

| Sample no. | Experimental conditions | *b*-Value at onset of AE | *b*-Value at failure | Peak AE hit rate ($min^{-1}$) |
|---|---|---|---|---|
| ST1 | Uniaxial and 25 ± 5 °C | 1.28 | 0.97 | 1993 |
| ST11 | Uniaxial and 25 ± 5 °C | 1.23 | 0.98 | 1323 |
| ST36 | Uniaxial and 300 ± 5 °C | 1.19 | 0.96 | 2576 |
| ST37 | Uniaxial and 300 ± 5 °C | 1.15 | 0.95 | 1396 |
| ST41 | Uniaxial and 600 ± 5 °C | 1.21 | 1.02 | 2915 |
| ST45 | Uniaxial and 900 ± 5 °C | 1.22 | 0.91 | 888 |
| ST33 | 10 MPa and 300 ± 5 °C | 1.11 | 1.01 | 306 |
| ST42 | 10 MPa and 600 ± 10 °C | 1.03 | 0.84 | 305 |
| ST14 | 30 MPa and 25 ± 5 °C | 1.20 | 0.67 | 1173 |
| ST15 | 30 MPa and 25 ± 5 °C | – | 1.02 | 269 |

*b*-Value at onset of AE is omitted when there were not enough AE events (<200) before the peak stress to calculate a reliable *b*-value. AE were not recorded on samples ST43, ST20, ST40, ST5 and ST34 due to use of a cooling system that masked the AE with too much noise.

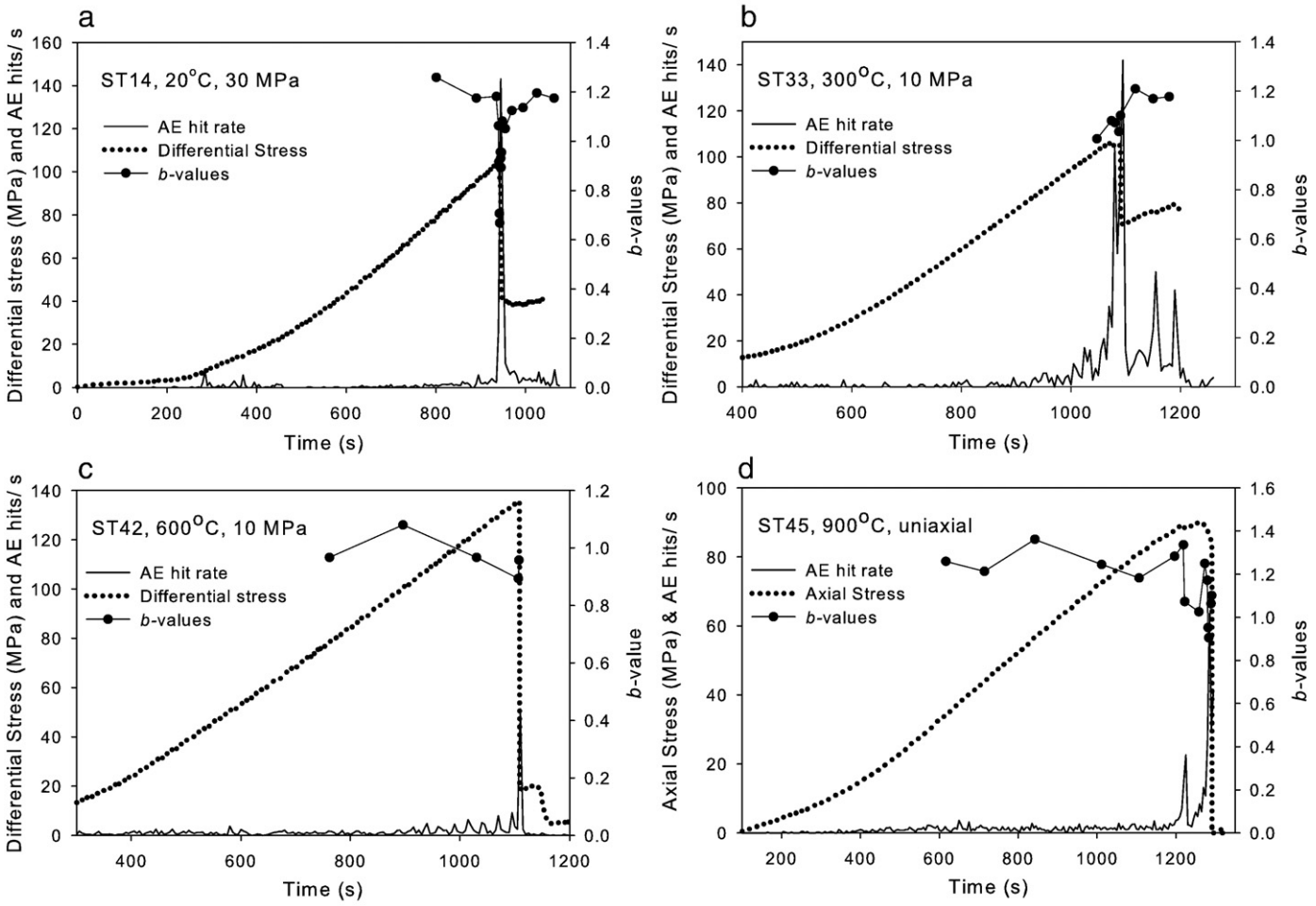


**Fig. 6.** Acoustic emission hits per second (calculated at 5 second intervals), *b*-values (calculated for 200 hits at 100 hit intervals) and differential axial stress plotted against time for a) sample ST14 deformed in triaxial compression with 30 MPa confining pressure at room temperature, b) sample ST33 deformed in triaxial compression with 10 MPa confining pressure at 300 °C, c) sample ST42 deformed in triaxial compression with 10 MPa confining pressure at 600 °C, and d) sample ST45, deformed in uniaxial compression at 900 °C.

### 5.2. Brittle–ductile deformation

The mode I, level I fracture toughness of ancestral Mount Shasta andesite increased slightly at higher temperatures (750 °C and 900 °C; Fig. 2). This may be caused by (1) blunting of crack tips due to melting of the glass phase in the groundmass and plasticity of the crystals, or (2) a greater amount of pre-existing thermal cracks, which increases the size of the crack tip process zone and so reduces the stress intensity at the crack tip. The fracture toughness results were less consistent at 900 °C, as were the strength and Young's Modulus in uniaxial and triaxial compression. This may be due to this temperature lying within the brittle–ductile transition for this rock; where its rheology changes rapidly with temperature. Within the brittle–ductile transition, a temperature increase of 50 °C can lead to a strength drop of 90% in dry andesite (Bauer et al., 1981). It is thus suggested that the strength variations at 900 °C may be attributed to small temperature variations and sample variability being heightened within the brittle ductile transition.

There was evidence of some ductile deformation of samples deformed in compression at 900 °C from their stress–strain curves, barrel shaped sample bulging, and the melt formation on their fracture surfaces. However, these samples still emitted a comparable amount of AE during their deformation and failure compared to the samples deformed from 25 to 600 °C (Table 2). It thus supports the theory of Tuffen and co-workers (Neuberg et al., 2006; Tuffen et al., 2008, 2003; Tuffen and Dingwell, 2005) that volcano-tectonic and hybrid earthquakes may originate within magma at eruptible temperatures if they are deformed at sufficiently high strain rates.

### 5.3. Use of mechanical data in eruption forecasting models

In existing models of rock fracture in volcanic systems, the stored bulk strain ($\sigma/Y$) and bulk strain energy per unit volume ($\sigma^2/Y$) in edifice and lava flow rocks (where $\sigma$ is the applied stress and $Y$ is the Young's Modulus) are key parameters for forecasting the expected eruption time (Kilburn, 2003; Kilburn and Sammonds, 2005) and lava flow dynamics (Kilburn, 2004). These values are calculated from experimentally determined values of $\sigma$, the differential stress at failure (in compression or tension), and $Y$, the Young's Modulus, of volcanic rocks. For eruption forecasting (Kilburn, 2003), these values were taken from uniaxial and triaxial experiments on Etnean trachybasalt (Rocchi et al., 2004). The stored bulk strain and bulk strain energy per unit volume at failure from all the andesite compression experiments presented in this paper and results for both Etnean trachybasalt and Vesuvian phono-tephrite published in Rocchi et al. (2004) are plotted against temperature in Fig. 7. The results for the bulk strain (Fig. 7a) indicate that the amount of recoverable strain at failure is (1) independent of temperature until the temperature reaches 900 °C, and (2) only weakly affected by differences in bulk chemical and petrographic composition among the samples presented here. At longer timescales the increase in strain could occur at lower temperatures due to transient creep. However, we note that strain rates in the final approach to volcanic eruptions are expected to be far higher than those typically considered for tectonic deformation (Tuffen et al., 2008), where transient creep is more important. The only sample with less accumulated bulk strain was from the crust of

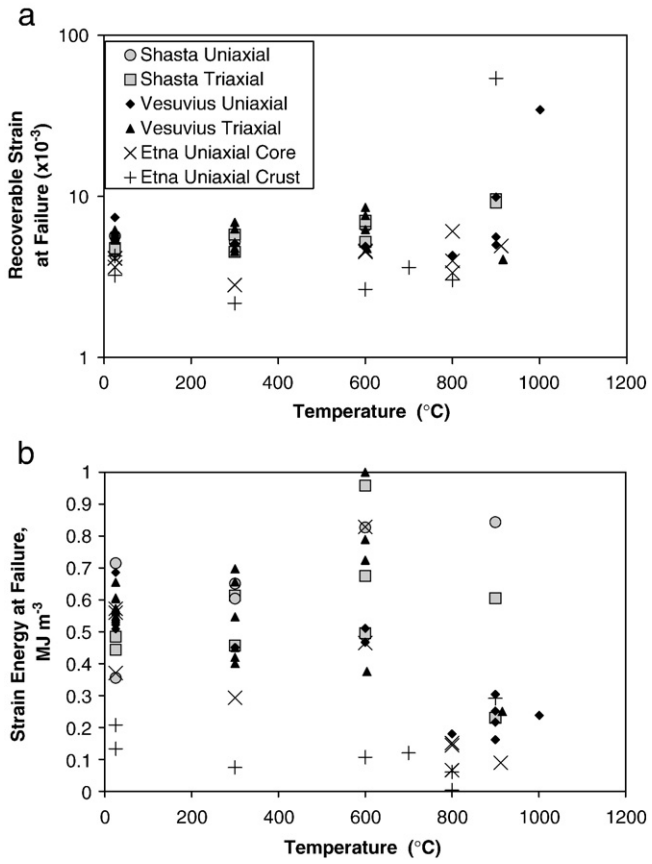


**Fig. 7.** Recoverable strain (a) and strain energy (b) at failure plotted against temperature for samples of andesite deformed in uniaxial and triaxial compression in this study and samples of Vesuvius and Etna lava flows deformed in uniaxial and triaxial compression in Rocchi et al. (2004).

the Etna lava flow. This sample had the highest porosity, which could result in sample failure after less accumulated strain. At higher temperatures, the increases in critical strain could be attributed to partial melting and increased mineral plasticity. The strain energy per unit volume (Fig. 7b), lies between 0.1 and 1 MJ m$^{-3}$ for most compositions and temperatures, with the Etna samples at all temperatures and all compositions at temperatures >800 °C defining the lower limit.

The expected VT event rate peaks ($dN_p/dt$) at andesitic, subduction zone volcanoes (such as Soufriere Hills, Montserrat and Pinatubo, Philippines) in the final acceleration before an eruption can be described as (Kilburn, 2003):

$$dN_p / d_t \propto \exp\left[K\left(\sigma^2 / Y\right)N\right] \quad (1)$$

where $K$ is a function of rock temperature, density, and molecular weight, expected to lie in the range $4.5 \pm 3.2 \times 10^{-3}$, and $N$ is the total number of events. This value also denotes the expected linear gradient in inverse event rates. Data from VT seismicity before the 1991 eruption of Pinatubo and the 1995 eruption of Soufriere Hills indicate values of $\sigma^2/Y$ ~0.1 MJ m$^{-3}$ (Kilburn, 2003). These are at the lower limit of the values in Fig. 7b, which is the value found for all temperatures of Etnean trachybasalt and all compositions at temperatures >800 °C. The low required values of $\sigma^2/Y$ thus suggest (1) that volcanic systems are characterized by zones of weakness through which fractures preferentially grow, and (2) that fracture propagation may be favoured by elevated temperatures of 800–900 °C in the host rock. Whilst the distribution of flaws and fractures in rocks is usually scale invariant, such that the effect of a microcrack on a laboratory sample is comparable to that of a macrocrack on a volcano, the selection of 'intact' samples for laboratory testing may result in laboratory samples appearing stronger than their behaviour in the field (Jaeger and Cook, 1976). This offers further support to the suggestion that zones of weakness control the behaviour of the volcanic edifice.

### 5.4. Acoustic emissions

A drop in $b$-value coincided with the failure of most samples (Table 2 and Fig. 6). This reflects an increase in the stress intensity at fracture tips as the crack lengths increase with the propagation of the macroscopic fracture (Main, 1991; Meredith and Atkinson, 1983). The $b$-values before and after sample failure for samples ST14 and ST42, were similar (Fig. 6a). This recovery could be attributed to (1) detected AE being dominated by cracking around the fault rather than movement along it, so that the AE are occurring in the same volume on the same faults before and after the formation of the macroscopic fracture, or (2) movements and asperities along the macroscopic fracture plane have the same size–frequency distribution as faults throughout the sample in general.

For the sample deformed in uniaxial compression at 900 °C (Fig. 6d), the $b$-value dropped to a local minimum at peak stress, and then recovered during strain softening deformation, before reaching a lower minimum as the sample failed. This $b$-value 'double minimum' has been observed previously and explained in terms of a fracture mechanics model for rock undergoing significant strain softening deformation before dynamic failure (Sammonds et al., 1992). This sample showed a comparable amount of AE to samples deformed at room temperature, providing further evidence for the claim that rocks deformed at a high strain rate at temperatures close to their melting point can fracture seismogenically (Tuffen et al., 2008).

Kilburn's (2003) multiscale fracture model for forecasting volcanic eruptions was applied to the AE hit rate data for sample ST45 (Fig. 8). In this model, the eruption or system failure time is forecast by extrapolating a linear trend in minima in inverse earthquake rates to zero. There were 2 swarms of AE during the deformation of this sample, one close to the peak stress that did not culminate in sample failure (1200 to 1230 s), and one during strain softening deformation culminating in macroscopic failure of the sample (1250 to 1290 s). For the first swarm, inverse rate minima could not be separated out from the other inverse rates, and the gradient was $1.04 \times 10^{-2}$ (Fig. 8). The 'failure forecast' from this was 60 s before the sample failed and the gradient was outside the limits expected in the model. For the second

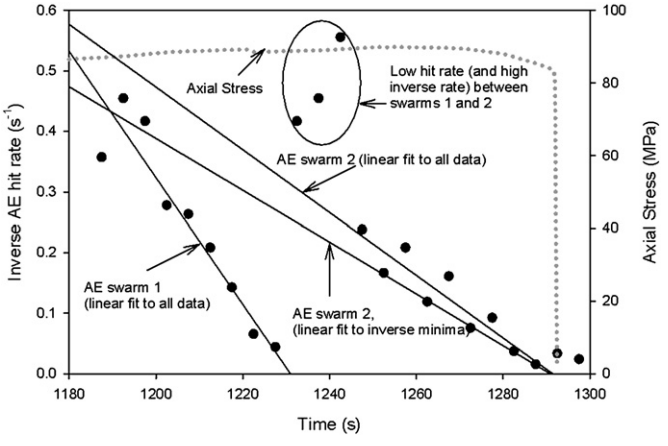


**Fig. 8.** Application of the multiscale fracture model to inverse hit rates during deformation of sample ST45, which failed at 1292 s. Minima could not be separated from other inverse rates for the first swarm of AE (from 1200 to 1230 s). The linear inverse rate gradient was $1.04 \times 10^{-2}$, with an $R^2$ value of 0.969 and a failure forecast time of 1231 s. For the second swarm of AE, the linear inverse rate gradient was $4.3 \times 10^{-3}$, with an $R^2$ value of 0.998 and a failure forecast time of 1291 s. For all AE in this swarm, the linear inverse rate gradient was $5.2 \times 10^{-3}$, with an $R^2$ value of 0.875 and a failure forecast time of 1291 s.

swarm, inverse rate minima could be selected, and gave an accurate forecast of the sample failure time, with a gradient of $4.3\times10^{-3}$, which is within the expected limits of the model. Extrapolation of the linear trend in all inverse rates in this second swarm also gave an accurate forecast and had a gradient within the expected limits ($5.2\times10^{-3}$). However, the $R^2$ value of this fit was much lower at 0.875 compared to 0.998 for inverse minima. The gradient for the AE swarm that resulted in sample failure agreed with the model and the inverse rate minima had a better linear fit than all inverse rates. This supports the model and hence also the idea that laboratory data can be used to interpret trends at field scale.

## 6. Conclusions

The mechanical properties of ancestral Mount Shasta andesite remained the same for temperatures up to 600 °C and confining pressures from atmospheric to 50 MPa in dry conditions. The Mode I fracture toughness is $2.5\pm0.5$ MPa $m^{1/2}$, the peak differential compressive stress is $110\pm30$ MPa; and Young's Modulus is $20\pm5$ MPa. The fracture toughness in wet conditions, which were tested at 150 and 200 °C, decreased by ~30%. The toughness increased by ~50% at temperatures of 750 °C and above. The compressive strength (the peak differential stress) and Young's Modulus both fell by ~50% at 900 °C. We therefore conclude that, within and immediately beneath a volcanic edifice, the strength and elasticity of andesitic country rock will not be affected by temperature or pressure unless within 10 s of m of active magma. However, the gradient of inverse seismic event rate minima seen before some volcanic eruptions, as interpreted with Kilburn's (2004) multiscale fracture model and mechanical data from this study, suggests that zones of weaker material or high temperatures control the rates of fracturing before eruptions.

A peak in AE hit rates coincided with macroscopic failure for all uniaxial and triaxial compression experiments for which AE were recorded. The acceleration in AE before sample failure is similar to that described for earthquakes before eruptions in forecasting models, supporting the use of laboratory data to interpret field trends. For most experiments of all types, sample failure also coincided with a minimum in the seismic *b*-value, which is expected when the stress intensity at fracture tips increases. The large amount of AE recorded during experiments at 900 °C provides further evidence for existing claims that seismogenic fracture can occur in eruptible magma (Tuffen et al., 2008). The formation of brittle shear fractures at this temperature offers further evidence that fracturing controls the dynamics of lava domes and magma conduits, given the comparable strain rates in the field and the laboratory.

## Acknowledgements

We are grateful to Steve Boon and John Bowles for help with the experimental apparatus and to Bill Hirt for help during fieldwork on Mount Shasta. We acknowledge the support of the UK Natural Environment Research Council. We are grateful for helpful comments from two anonymous reviewers.

## Appendix A. Supplementary data

Supplementary data associated with this article can be found, in the online version, at doi:10.1016/j.epsl.2009.01.032.

## References

Aki, K., 1965. Maximum likelihood estimate of b in the formula log N = a-bM and its confidence limits. Bull. Earthqu. Res. Inst. 43, 237–239.
Aspinall, W.P., Miller, A.D., Lynch, L.L., Latchman, J.L., Stewart, R.C., White, R.A., Power, J.A., 1998. Soufriere Hills eruption, Montserrat, 1995–1997: volcanic earthquake locations and fault plane solutions. Geophys. Res. Lett. 25, 3397–3400.
Balme, M.R., Rocchi, V., Jones, C., Sammonds, P.R., Meredith, P.G., Boon, S., 2004. Fracture toughness measurements on igneous rocks using a high pressure, high temperature rock fracture mechanics cell. J. Volcanol. Geotherm. Res. 132, 159–172.
Bauer, S.J., Friedman, M., Handin, J., 1981. Effects of water saturation on strength and ductility of three igneous rocks at effective pressures to 50 MPa and temperatures to partial melting. Proc. 2nd Symp. Rock Mechanics, pp. 79–84.
Beeler, N.M., Mastin, L.G., Roeloffs, E., Gerlach, T.M., 2005. Possible role of sliding friction in controlling the 2004–2005 Mount St Helens eruption. Eos Trans. AGU 86 Fall Meet. Suppl., Abstract. V53D-1596.
Cox, S.J.D., Meredith, P.G., 1993. Microcrack formation and material softening in rock measured by monitoring acoustic emissions. Int. J. Rock Mech. Min. Sci. 30 (1), 11–24.
Denlinger, R.P., 1990. A model for dome eruptions at Mount St Helens, Washington based on subcritical crack growth. In: Fink, J.H. (Ed.), Lava Flows and Domes: Emplacement Mechanisms and Hazard Implications. Springer Verlag, pp. 70–87.
Fink, J.H., Malin, M.C., Anderson, S.W., 1990. Intrusive and extrusive growth of the Mount St Helens lava dome. Nature, 348, 435–437.
Fredrich, J.T., Wong, T.-F., 1986. Micromechanics of thermally induced cracking in three crustal rocks. J. Geophys. Res. 91, 12743–12764.
Fremont, M.J., Malone, S.D., 1987. High-precision relative locations of earthquakes at Mount St-Helens, Washington. J. Geophys. Res. 92, 10223–10236.
Friedman, J.D., Olhoeft, G.R., Johnson, D.R., Frank, D., 1981. Heat content and thermal energy of the June dacite dome in relation to total energy yield, May–October 1980. In: Lipman, P.W., Mullineaux, D.R. (Eds.), The 1980 eruptions of Mount St Helens, Washington. U.S. Geol. Surv. Prof. Paper, 1250, pp. 557–567.
Friedman, M., Handin, J.N., Higgs, G., Lantz, J.R., 1979. Strength and ductility of four dry igneous rocks at low pressures and temperatures to partial melting. Proc. Symp. Rock Mechanics 35–50.
Grove, T.L., Baker, M.B., Price, R.C., Parman, S.W., Elkins-Tanton, L.T., Chatterjee, N., Muntener, O., 2005. Magnesian andesite and dacite lavas from Mt. Shasta, northern California: products of fractional crystallization of $H_2O$-rich mantle melts. Contr. Min. Pet. 148, 542–565.
Hacker, B.R., Christie, J.M., 1991. Experimental deformation of a glassy basalt. Tectonophys 200, 79–96.
Hale, A.J., Wadge, G., 2003. Numerical modelling of the growth dynamics of a simple silicic lava dome. Geophys. Res. Lett. 30, art–2003.
Irwin, G.R., 1958. Fracture. In: Flugge, S. (Ed.), Handbuch der Physik 6. Springer, Berlin, pp. 551–590.
ISRM, C.o.T.M., 1988. Suggested methods for determining the fracture toughness of rock. Int. J. Rock Mech. Min. Sci. Geomech. Abstr. 25, 71–97.
Jaeger, J.C., Cook, N.G.W., 1976. Fundamentals of Rock Mechanics. Chapman and Hall, London.
Kelley, F.R., Wagner, D.L., Saucedo, G.J., 1987. Radiometric ages of rocks in the Weed quadrangle, California, booklet to accompany the regional geologic map series Weed quadrangle-map no. 4A (geology). California Department of Conservation. Division of Mines and Geology, Sacramento.
Kilburn, C.R.J., 1996. Patterns and predictability in the emplacement of subaerial lava flows and flow fields. In: Scarpa, R., Tilling, R.I. (Eds.), Monitoring and Mitigation of Volcano Hazards. Springer, Berlin, pp. 491–537.
Kilburn, C.R.J., 2003. Multiscale fracturing as a key to forecasting volcanic eruptions. J. Volcanol. Geotherm. Res. 125, 271–289.
Kilburn, C.R.J., 2004. Fracturing as a quantitative indicator of lava flow dynamics. J. Volcanol. Geotherm. Res. 132, 209–224.
Kilburn, C.R.J., Sammonds, P.R., 2005. Maximum warning times for imminent volcanic eruptions. Geophys. Res. Lett. 32, art–L24313.
Kilburn, C.R.J., Voight, B., 1998. Slow rock fracture as eruption precursor at Soufriere Hills volcano, Montserrat. Geophys. Res. Lett. 25, 3665–3668.
Lore, J., Gao, H., Aydin, A., 2000. Viscoelastic thermal stress in cooling basalt flows. J. Geophys. Res. 105, 23695–23709.
Main, I.G., 1987. A characteristic earthquake model of the seismicity preceding the eruption of Mount St. Helens on 18 May 1980. Phys. Earth Planet. Int. 49, 283–292.
Main, I.G., 1991. A modified Griffith criterion for the evolution of damage with a fractal distribution of crack lengths: application to seismic event rates and *b*-values. Geophys. J. Int. 107, 353–362.
Main, I.G., Sammonds, P.R., Meredith, P.G., 1993. Application of a modified Griffith criterion to the evolution of fractal damage during compressional rock failure. Geophys. J. Int. 115, 367–380.
McGuire, W., Kilburn, C.R.J., 1997. Forecasting volcanic events: some contemporary issues. Geol. Rundsch. 86, 439–445.
McNutt, S.R., 2005. Volcanic seismology. Ann. Rev. Earth Planet. Sci. 33, 461–491.
Meredith, P.G., Atkinson, B.K., 1985. Fracture toughness and subcritical crack growth during high-temperature tensile deformation of westerly granite and black gabbro. Phys. Earth Planet. Int. 39, 33–51.
Meredith, P.G., Atkinson, B.K., 1983. Stress corrosion and acoustic emission during tensile crack propagation in Whin Sill dolerite and other basic rocks. Geophys. J. Roy. Astr. Soc. 75, 1–21.
Meredith, P.G., Main, I.G., Jones, C., 1990. Temporal variations in seismicity during quasi-static and dynamic rock failure. Tectonophys. 175, 249–268.
Murrell, S.A.F., Chakravarty, S., 1973. Some new rheological experiments on igneous rocks at temperatures up to 1120 °C. Geophys. J. Roy. Astr. Soc. 34, 211–250.
Nakada, S., Shimizu, H., Ohta, K., 1999. Overview of the 1990–1995 eruption at Unzen Volcano. J. Volcanol. Geotherm. Res. 89, 1–22.
Neuberg, J., Tuffen, H., Collier, L., Green, D., Powell, T., Dingwell, D., 2006. The trigger mechanism of low-frequency earthquakes on Montserrat. J. Volcanol. Geotherm. Res. 153, 37–50.

Nishizawa, O., Onai, K., Kusunose, K., 1984. Hypocenter distribution and focal mechanism of AE events during 2-stress stage creep in Yugawara Andesite. Pure Appl. Geophys. 122, 36–52.
Paterson, M.S., 1978. Experimental Rock Deformation — the Brittle Field. Springer-Verlag, Berlin, pp. 33–39.
Rao, M.V.M.S., Kusunose, K., 1995. Failure zone development in andesite as observed from acoustic-emission locations and velocity changes. Phys. Earth Planet. Int. 88, 131–143.
Rocchi, V., 2002. Fracture of Basalts under Simulated Volcanic Conditions. Unpublished Ph.D. thesis, University of London (UCL).
Rocchi, V., Sammonds, P.R., Kilburn, C.R.J., 2002. Flow and fracture maps for basaltic rock deformation at high temperatures. J. Volcanol. Geotherm. Res. 120, 25–42.
Rocchi, V., Sammonds, P.R., Kilburn, C.R.J., 2004. Fracturing of Etnean and Vesuvian rocks at high temperatures and low pressures. J. Volcanol. Geotherm. Res. 132, 137–157.
Roman, D.C., Neuberg, J., Luckett, R.R., 2006. Assessing the likelihood of volcanic eruption through analysis of volcano-tectonic earthquake fault-plane solutions: Earth Planet. Sci. Lett. 248, 244–252.
Rust, A.C., Manga, M., Cashman, K.V., 2003. Determining flow type, shear rate and shear stress in magmas from bubble shapes and orientations. J. Volcanol. Geotherm. Res. 122, 111–132.
Sammonds, P.R., Meredith, P.G., Main, I.G., 1992. Role of pore fluids in the generation of seismic precursors to shear fracture. Nature 359, 228–230.
Scandone, R., Cashman, K., Malone, S.D., 2007. Magma supply, magma ascent and the style of volcanic eruptions. Earth Planet. Sci. Lett. 253, 513–529.
Smith, J.V., Miyake, Y., Oikawa, T., 2001. Interpretation of porosity in dacite lava domes as ductile–brittle failure textures. J. Volcanol. Geotherm. Res. 112, 25–35.
Smith, R., 2006. Rates of rock fracturing as a tool for forecasting eruptions at andesitic–dacitic stratovolcanoes. Unpublished Ph.D. thesis, University of London (UCL).
Smith, R., Kilburn, C.R.J., Sammonds, P.R., 2007. Rock fracture as a precursor to lava dome eruptions at Mount St Helens from June 1980 to October 1986. Bull. Volcanol. 69, 681–693.
Takanohashi, M., Takahashi, H., 1986. Evaluation of rock fracture toughness using the AE technique — effect of the lithologic character of rocks on fracture toughness. Progr. Acoust. Em. III, 357–364.
Thompson, B.D., Young, R.P., Lockner, D.A., 2006. Fracture of Westerly granite under AE feedback and constant strain rate loading: nucleation, quasi-static propagation, and the transition to unstable fracture propagation. Pure App. Geophys. 163, 995–1019.
Tuffen, H., Dingwell, D., 2005. Fault textures in volcanic conduits: evidence for seismic trigger mechanisms during silicic eruptions. Bull. Volcanol. 67, 370–387.
Tuffen, H., Dingwell, D.B., Pinkerton, H., 2003. Repeated fracture and healing of silicic magma generate flow banding and earthquakes? Geology 31, 1089–1092.
Tuffen, H., Smith, R., Sammonds, P.R., 2008. Evidence for seismogenic fracture of silicic magma. Nature 453, 511–514.
Voight, B., 1988. A Method for prediction of volcanic eruptions. Nature 332, 125–130.
Voight, B., Elsworth, D., 1997. Failure of volcano slopes. Geotech 47, 1–31.
Waza, T., Kurita, K., Mizutani, H., 1980. The effect of water on the subcritical crack growth in silicate rocks. Tectonophys 67, 25–34.
Winter, J.W., 2001. An Introduction to Igneous and Metamorphic Petrology. Prentice-Hall Inc., Upper Saddle River, New Jersey.